Methane emissions from a sediment-deposited island in a Lancang-Mekong reservoir: Spatial heterogeneity and mechanisms

Wenqing Shi[1,2], Qiuwen Chen[1,2], Jianyun Zhang[1,3], Cheng, Chen[2], Yuchen Chen[2],Yuyu Ji[2,4], Juhua Yu[1,2], Bryce R. Van Dam[5]

[1]State Key Laboratory of Hydrology-Water Resources & Hydraulic Engineering, Nanjing Hydraulic Research Institute, China

[2]Center for Eco-Environment Research, Nanjing Hydraulic Research Institute, China

[3]Research Center for Climate Change, Ministry of Water Resources, China

[4]College of Water Conservancy and Hydropower Engineering, Hohai University, China

[5]Institute of Marine Sciences, University of North Carolina at Chapel Hill, USA

Correspondence to: Qiuwen Chen (qwchen@nhri.cn)

Abstract

In dammed rivers, sediment accumulation creates potential methane emission hotspots, which have been extensively studied in forebays. However, methane emissions from sidebays remain poorly understood. We investigated methane emissions from a sediment-deposited island situated in the sidebay of the Manwan Reservoir, Lancang-Mekong River. High methane emissions (maximum 10.4 mg $h^{-1}m^{-2}$) were observed at the island center, while a ring-like zone of low-to-negative methane emission was discovered at the drawdown area around the island edge, whose flux varied between -0.2–1.6 mg $h^{-1}m^{-2}$. The ring-like zone accounted for 89.1 % of the island area, of which 9.1 % was a methane sink zone. Microbial processes in the drawdown area, regulated by hydrological variations, were responsible for the low methane flux in this area. Under reservoir operation, frequent water level fluctuations enhanced hyporheic exchange and created oxygen gradients along the hyporheic flow path. Dissolved oxygen in hyporheic water decreased from 4.80 mg L^{-1} at the island bank edge to 0.43 mg L^{-1} at the center, which in turn decreased methanogen abundance for methane production and increased methanotroph abundance for methane oxidation at the ring-like zone. This study quantified the methane emissions from sediment deposited islands in the reservoir and helps to evaluate the global warming effects of hydropower systems.

1 Introduction

Natural rivers form continuous ecosystems, in which physical and chemical factors drive biological processes from headwaters to river deltas (Butman and Raymond, 2011; Wilkinson et al., 2015). Along this continuum, rivers receive terrestrial organic carbon (OC) and deliver it to the ocean at a global average rate of approximately 400–900 Tg OC per year (Butturini et al., 2016; Seitzinger et al., 2005; Ran et al., 2013). In the past two decades, many rivers have become intensively regulated by dams for a variety of purposes, including improved navigation, water supply, flood control, and hydropower production (Maavara et al., 2015). These engineering works decrease water velocity, converting rivers into a series of lentic reservoirs, where sediment accumulates in forebays and sidebay islands (Maeck et al., 2013). Globally, the sediment accumulation process has reduced the river-to-ocean flux of terrestrial OC by 26 % (Syvitski et al., 2005).

Methane is the second most important greenhouse gas, contributing approximately 18 % to total global warming effects (Smith et al., 2013; Wuebbles and Hayhoe, 2002). Inland waters (lakes, rivers, and reservoirs) are significant sources of atmospheric methane, which is mainly released from anoxic sediment (Bastviken et al., 2011; Sobek et al., 2012). After river damming, settling particles aggregate to form cohesive sediment layers, which often become anoxic after oxygen is consumed but not replenished through diffusive exchange (Rubol et al., 2013; Maeck et al., 2013). Subsequently, large amounts of methane may be produced and released into the atmosphere (Thornton et al., 1990; Maeck et al., 2013; Wilkinson et al., 2015), thereby

reducing the green credentials of hydropower. This issue has received considerable attention in dammed rivers (Giles, 2006; Hu and Cheng, 2013). Maeck et al. (2013) identified reservoirs as methane emission hotspots by comparing reservoir and riverine reaches, and estimated that global methane emissions have increased by 7 % due to sedimentation in dammed rivers. In sidebays, the deposited sediments often created the drawdown area under water level fluctuations, where water, heat, nutrients and chemicals are exchanged and many biogeochemical reactions preferentially occur (Tonina and Buffington, 2011; Cardenas and Markowski, 2010), potentially emitting large amounts of greenhouse gases. Previous studies have mainly focused on methane emissions from dam forebays (Yang et al., 2013; DelSontro et al., 2010; DelSontro et al., 2011), while the understandings of methane emissions from sediments deposited in sidebays remain poor.

In reservoirs, the water level decreases during hydropower production, and increases with the inputs from inflows during the stagnant hydropower production. As a result, the water level frequently fluctuates following hydropower production demands, which enhances hyporheic exchange by driving water flow in and out of the drawdown area (Tonina and Buffington, 2011; Hucks Sawyer et al., 2009). This may lead to changes of oxygen conditions in the interior of the drawdown area. Zarnetske found a redox gradient along the hyporheic flow paths in a third-order stream in the Willamette River basin, USA (Zarnetske et al., 2011a). Methane from sediments is mainly produced by methanogens, and is consumed by methanotrophs (Borrel et al., 2011). Methanogens and methanotrophs belong to anaerobic and aerobic microbes, respectively (Nazaries et

al., 2013). The oxygen conditions in sediments have been found to manipulate these microbial processes and methane emission (Chamberlain et al., 2016; Shi et al., 2018). Hence, we suppose the changes of oxygen conditions in sediments may alter methane emission scheme on sediment-deposited islands in reservoir sidebays.

In this study, methane emissions from a sediment-deposited island were investigated in the sidebay of Manwan Reservoir, Lancang-Mekong River. Monitoring wells were established to probe hyporheic exchange and oxygen gradients across the island. Methanogen and methanotroph abundances in the sediment were analyzed using quantitative polymerase chain reaction (qPCR) to reveal the associated molecular mechanism. The objective of this study was to explore methane emission patterns from sediment-deposited zones in the reservoir sidebay and the underlying mechanisms.

2 Methods

2.1 Study area

The Lancang-Mekong River is a trans-boundary river in Southeast Asia and the tenth-largest river in the world, which originates from the Tibetan Plateau in China, continues into Myanmar, Lao PDR, Thailand, Cambodia and Viet Nam, and discharges into the South China Sea. It has a length of approximately 4909 km, a total watershed area of 795,000 km^2 (Mekong River Commission, 2018). Due to rich hydropower resources, cascade dams have been built on the mainstream of the Lancang-Mekong River. After impoundment, about 33 sediment-deposited islands of 4.3×10^5 m^2 formed in the reservoir sidebay in the upstream section of the Lancang-Mekong River in China, of

which 81.8% are located at the convex bank, and 18.2% at the concave bank (Fig. S1). This study selected the widely distributed type of island at the convex bank for investigation, which is located in the Manwan Reservoir (24°43′44″ N, 100°23′5″ E). The studied island has an oval shape with a surface area of 1.3 × 10^4 m^2 (Fig. 1). Manwan dam is the first-built one (completed in 1993) in the upstream section of the Lancang-Mekong River in China, with a height of 132 m. The Manwan Reservoir has a normal water level of 994 m, a total storage capacity of 5.0 × 10^8 m^3, an installed capacity of 1.5 × 10^6 kW and hydrological residence time of 0.78 a. Manwan has a subtropical plateau monsoon climate, and the temperature features no distinct seasons. Under water level fluctuation induced by reservoir operation, the island bank is frequently flooded (Fig. S2).

2.2 Monitoring wells

Ten monitoring wells were installed in the island bank at 0.5 (W1), 1.5 (W2), 3.5 (W3), 6.5 (W4), 10.5 (W5), 15.5 (W6) 20.5 (W7), 25.5 (W8), 30.5 (W9), and 35.5 m (W10) from the waterline, respectively (Fig. S2). The wells were 90-mm diameter perforated polyvinylchloride pipes, reaching a depth of 2.0 m below the ground surface. To prevent flooding, the wells were extended 2.0 m aboveground. Due to hydropower production, the reservoir runs in a pseudo-periodic hydrological regime with cyclic water level fluctuations. Here, we monitored a complete cycle of water level fluctuation within 115 h. Water levels were measured every 10 min from 11 to 16 September 2016 using automated water level recorders (U2000101, OneSetHoBo, USA), which were mounted at the bottom of W5, W7, W10, and the reservoir (Fig. S3).

Instantaneous lateral fluid fluxes (q) across the island bank per unit length were calculated following the Darcy Eq. (1) (Gerecht et al., 2011; Hucks Sawyer et al., 2009):

$$q(t) = -Kb \cdot \left[\frac{\vartheta h(x,t)}{\vartheta x}\right] \quad (1)$$

where Kb is sediment transmissivity, m d^{-1}; h is hydraulic head, m; x is distance, m; and t is time, d. A positive q value indicates flow from the reservoir to the island. The island Kb was 0.99 m d^{-1}, which was measured according to Philip (1993).

2.3 Sampling and physicochemical analysis

After water level receded at the monitoring time of 100 h, groundwater (100 ml) was carefully sampled in triplicate from each monitoring well with a portable peristaltic pump (SC-1/253Yx, Chongqing Jieheng Peristaltic Pump Co., Ltd., China), and then filtered *in situ* using portable syringe filters for water DOC analysis. Sediment (5 g) was synchronously collected in triplicate from 10 cm below the surface adjacent to each well (Fig. 1b) using a hand shovel, and then quickly homogenized before the storage in the plastic ziplock bag for the analyses of sediment OC and microbe. At a reservoir site adjacent to W1, water and surface sediment samples were also collected in triplicate using a stainless-steel bucket and an Ekman grab sampler, respectively. The collected water and sediment samples were kept frozen in an ice box (-5 ℃–-10 ℃) and transported to the laboratory for analysis within three days.

Dissolved oxygen (DO) in the reservoir was measured using a multi-sensor probe (YSI 6600, Yellow Springs Instruments, USA), and the DO at each well was measured *in situ* using a DO meter (JPB-607A, Shanghai INESA Scientific Instrument Co. Ltd., China) by directly placing the probe in the well. Analysis of dissolved organic carbon

(DOC) in the water was conducted on filtered samples (Whatman GF/F, UK) using a total organic carbon analyzer (Liqui TOC II, Elementar Inc., Germany). Sediment OC was determined using a vario MACRO cube elementar (Elementar Inc., Germany). Fresh sediment was freeze-dried and ground before analysis. Approximately 30 mg of each sample was weighed in a tin cup and acidified with two drops of 8 % H_3PO_4 to remove inorganic carbonates before OC analysis.

2.4 Methane flux analysis

Methane fluxes from the reservoir (eight sampling sites) and island (seventeen sampling sites) were analyzed using the static chamber method (Duchemin et al., 1999). The static chamber method has been widely used in the analyses of methane fluxes from air-soil/water interfaces, including the low-to-negative methane flux analyses (Veldkamp et al., 2013; Wang et al., 2013). The sampling sites are shown in Fig. 1b and Fig. S4. The plexiglass chamber consisted of a 6.28-L cylinder (20 cm in diameter, 20 cm in height) and a removable Styrofoam collar, and was covered with Mylar paper to prevent temperature rise inside the chamber when exposed to the sun. During gas collection in the reservoir, the chamber was fitted with the Styrofoam collar, which maintained the upper closed portion of the chamber about 10 cm above the water surface (Fig. S5). The outlet of the chamber was open during the chamber deployment, and was left to stand for 20 min to equilibrate with ambient pressure outside before sample collection. During gas collection on the island, the chamber was carefully inserted 5 cm deep into the sediment according to (Smith et al., 2000), leaving 15 cm above the sediment surface. The outlet of the chamber was also open during the

chamber deployment, and was left to stand for 90 min to equilibrate before sample collection. Gas samples (20 ml) were collected every 10 min over a 40-min period using a 25-ml polypropylene syringe and injected into a 12-ml pre-evacuated Exetainer® vial (839 W, Labco, UK) with double wadded septa caps for storage until analysis using a gas chromatograph (7890B, Agilent Technologies, USA). Exetainer® vials have been evaluated for storage of gas samples and they can limit sample loss to insignificant amounts for at least 3 months (Glatzel and Well, 2008; Van Dam et al., 2018). Gas fluxes were calculated using linear regression based on the concentration changes of five samples over time. Linear regression correlation coefficients of less than 0.95 were not accepted for further calculations (Duchemin et al., 1999). Methane fluxes at each site were measured in triplicate by placing three individual chambers. Simple spline interpolation was used to interpolate the methane emissions from the sampling sites into space in the reservoir and island separately (Immerzeel et al., 2009), and the range of the uncertain was 0.05 mg h^{-1} m^{-2}. Methane emission areas at eight different categories were also calculated in the island.

2.5 Microbial abundance analysis

After being transported to the laboratory, the frozen sediment samples were stored immediately at -80 ℃ for further molecular analysis. The sediment methanogens and methanotrophs adjacent to each monitoring well across the island (ten sediment samples) were quantified using qPCR. DNA extraction was undertaken using a FastDNA Power-Max Soil DNA Isolation Kit (MP Biomedical, USA) according to the manufacturer's instructions. The qPCR assay was performed using primers targeting methanogenic

archaeal 16S rDNA (primer set, 1106F/1378R) and methanotrophic *pmoA* genes (primer set, A189F/M661R) (Watanabe et al., 2007; Ma and Lu, 2011). Gene copies were amplified and quantified in a Bio-Rad cycler equipped with the iQ5 real-time fluorescence detection system and software (version 2.0, Bio-Rad, USA). All reactions were completed in a total volume of 20 μL containing 10 μL SYBR® *Premix Ex Taq*^{TM} (Toyobo, Japan), 0.5 mM of each primer, 0.8 μL of BSA (3 mg mL^{-1}, Sigma, USA), ddH_2O, and template DNA. The qPCR program mainly depends on the sequence and length of functional genes and primers used, and different qPCR programs for archaeal 16S rDNA and *pomA* were applied in this study. The qPCR program for archaeal 16S rDNA was as follows: 95 ℃ for 60 s, followed by 40 cycles of 95 ℃ for 25 s, 57 ℃ for 30 s, and 72 ℃ for 60 s, and the qPCR program for *pomA* referred to: 95 ℃ for 60 s, followed by 40 cycles of 95 ℃ for 25 s, 53 ℃ for 30 s, and 72 ℃ for 60 s. A standard curve was established by serial dilution (10^{-2}–10^{-8}) of known concentration plasmid DNA with the target fragment. All PCRs were run in triplicate on 96-well plates (Bio-Rad, USA) sealed with optical-quality sealing tape (Bio-Rad, USA). Three negative controls without the DNA template were included for each PCR run.

2.6 Data analysis

One-way analysis of variance (ANOVA) was employed to test the statistical significance of differences between sampling sites. Post-hoc multiple comparisons of treatment means were performed using the Tukey's least significant difference procedure. All statistical calculations were performed using the SPSS (v22.0) statistical package for personal computers. The level of significance was $P < 0.05$ for all tests.

206 ## 3 Results

207 ### 3.1 Physicochemical characteristics

208 As shown in Fig. 2, the island groundwater had lower DO but higher DOC, compared
209 with that of the bulk reservoir water. Lateral gradients of groundwater DO and DOC
210 were observed in the island. From the island edge to the center, DO and DOC decreased
211 significantly from 50.7 ± 2.0 to 4.5 ± 0.9% and 7.30 ± 0.54 to 1.70 ± 0.39 mg L^{-1},
212 respectively ($P < 0.05$) (Fig. 2a,b). In general, sediment OC was higher near the island
213 edge, decreasing from 6.37 ± 0.69 mg g^{-1} at the edge to 2.42 ± 0.60 mg g^{-1} at the center
214 of the island. Sediment OC in the reservoir was 6.63 ± 0.09 mg g^{-1} (Fig. 2c).

215 ### 3.2 Water level fluctuation and hyporheic exchange

216 The reservoir stage fluctuated frequently during the field survey, showing three distinct
217 peaks, with a maximum of 3.80 m in the first 37 h and gradual decline to below 1.30 m
218 in the next 60 h, yielding a maximum oscillation of 2.54 m. Similar oscillations were
219 observed in the island water table, but were damped and lagged relatively to the
220 reservoir stage fluctuations (Fig. 3a). In W5, W7, and W10, the water levels reached
221 3.27, 3.41, and 3.33 m, then fell to 1.74, 2.09, and 2.01 m, for a maximum oscillation
222 of 1.53, 1.33, and 1.32 m, respectively. Data from the automated water level recorders
223 indicated that the water level responses in W5, W7, and W10 lagged the reservoir stage
224 by 20, 25, and 30 min, respectively. Lateral hyporheic exchanges across the island bank
225 were calculated according to the Darcy Law, showing that the flux was largest at the
226 island edge and decreased from the edge to the center. The water exchange across the
227 0–10.5 m island edge zone was 1.2 and 4.7 times higher than those across the 10.5–20.5

m and 20.5–35.5 m zones, respectively. The flow rates at the reservoir-W5, W5-W7, and W7-W10 zones were relatively consistent at -0.55–1.35, -0.89–0.28, and -0.39–0.17 m^2 d^{-1} (Fig. 3b), resulting in a water exchange volume of 2.61, 2.26, and 0.56 m^3, respectively, over the 115-h observation period.

3.3 Methane emissions

High methane emission rates were observed at the island center, with a maximum of 10.4 mg $h^{-1}m^{-2}$. However, a ring-like zone of low-to-negative methane emission appeared at the drawdown area around the island edge, where the methane flux was maintained at -0.2–1.6 mg $h^{-1}m^{-2}$ (Fig. 4a). The negative flux values also suggest the occurrence of a methane sink at the island edge. The ring-like zone accounted for 89.1 % of the island area, of which 9.1 % accounted for the methane sink zone (Fig. 4b). Methane emissions were estimated to 8.3 and 5.4 g h^{-1} in total from the island center and the ring-like zone, accounting for 60.6% and 39.4%, respectively. Compared with the island, the methane flux from the adjacent reservoir was moderate at 0.4–5.5 mg $h^{-1}m^{-2}$ (Fig. 4a).

3.4 Methanogen and methanotroph abundances

Methanogens and methanotrophs were distributed non-uniformly across the island. In general, methanogen counts were low at the island edge but high at the center, whereas methanotrophs were abundant at the island edge but scarce in the center. From the island edge to the center, the methanogenic archaeal 16S rDNA gene increased from 0.12 × 10^5 to 5.34 × 10^5 copies g^{-1}, and the methanotrophic *pmoA* gene decreased from 1.57 × 10^6 to 0.64 × 10^6 copies g^{-1} (Fig. 5a). The ratio of methanogen to methanotroph

abundance increased from 0.01 at the island edge to 0.83 at the center (Fig. 5b).

4 Discussion

4.1 Hyporheic exchange and oxygen gradients

In hydropower reservoirs, the release of water pulses is often employed to increase power production and meet daily electricity peak demand (Bonalumi et al., 2012; Toffolon et al., 2010). Such hydropeaking creates daily water level fluctuations in the reservoir. In this study, frequent water level fluctuations were observed within the 115-h observation period, with a maximum of 3.80 m (Fig. 3a). In presence of head gradients and sediment resistance (Gerecht et al., 2011), a hysteretic response occurred in the island bank water table (Fig. 3a), driving water exchange between the reservoir and island (Fig. 3b). The water exchange flux was largest close to the island edge and decreased from the edge to the center, as water table fluctuations were attenuated (Fig. 3a).

During a storage-release cycle, the island switched from water gaining to losing at daily or hourly scales, creating a ring-like drawdown area of enhanced hyporheic exchange around the island. The drawdown area extended tens of meters into the island bank (Fig. 3b). If the river system was unregulated, however, hydrodynamics within the drawdown area would likely exhibit seasonal or annual patterns, or keep pace with snowmelt and rainstorm events, under a natural base flow-fed regime. In this case, the drawdown area may be limited or altogether absent (Boano et al., 2008; Cardenas and Wilson, 2007).

Exchange across the sediment-water interface involves mixing of surface water and groundwater through hyporheic flow (Hester et al., 2013; Naranjo et al., 2015). In this study, when the reservoir water entered the hyporheic flow path, it was typically rich in oxygen (Fig. 2d). As oxygen was consumed through aerobic respiration, other terminal electron acceptors were utilized (Klupfel et al., 2014), creating an oxygen gradient along the hyporheic flow path (Fig. 2d). This caused the spatial heterogeneity of the abundances of oxygen-sensitive methanogens and methanotrophs across the island. The oxygen-rich environment at the island edge favored methanotroph growth and inhibited methanogen growth, while the oxygen-poor environment at the island center inhibited methanotroph growth and favored methanogen growth. As a result, we detected low methanogen abundance at the island edge, but high abundance at the center, with methanotrophs showing the opposite pattern (Fig. 5).

4.2 Spatial heterogeneity of methane emissions

In dammed rivers, riverbed sediment accumulation creates potential methane emission hotspots. In this study, however, high methane emissions were only observed at the island center, with a ring-like low methane emission zone or even methane sink appearing around the island edge (Fig. 4a). This was attributed to the spatial heterogeneity of methanogens and methanotrophs across the island (Fig. 5), leading to an increase in methane production and a decrease in methane consumption from the island edge to the center. The methane sink at the island edge (Fig. 4) was mainly attributed to the strong oxidation by methanotrophs, which may consume methane to below equilibrium with the atmosphere. Methane emissions may not only rely on

bacterial abundance but also bacterial activity (Schwarz et al., 2008). This deserves further studies using other molecular biology techniques, such as DNA/RNA-based stable isotope probing (Dumont and Murrell, 2005). In addition, groundwater DOC and sediment OC at the island edge, which are carbon sources for methane emission, were higher than that at the island center (Fig. 2b,c), suggesting that both sediment heterogeneity and dilution effects of hyporheic exchange had limited contribution to the spatial pattern of methane emissions in the island.

4.3 Implications

Greenhouse gas emissions significantly detract from the green credentials of hydropower, and have thus received considerable research attention (Giles, 2006; Hu and Cheng, 2013). Previous studies have revealed that damming causes significant retention of carbon and creates deep, anoxic sediment strata, fueling methanogenesis and net water-air methane flux (Maeck et al., 2013). This study demonstrated that methane emissions at the most area of the sediment-deposited island were generally lower than the adjacent reservoir under water level fluctuation induced by reservoir operation (Fig. 4a), but higher than the drawdown area at other reservoir bank (-0.08–0.66 mg $h^{-1}m^{-2}$), such as Three Gorge Reservoir (Chen et al., 2011). This was mainly due to the deep sediment strata (about 60 m in depth) in the island. Given the widely distributed sediment-deposited islands in reservoirs, it should be of concern in future estimations of greenhouse gas emissions from dammed rivers.

Until now, few studies have concentrated on organic carbon mineralization in the drawdown area in reservoirs, with most focusing on the process of denitrification

316 (Zarnetske et al., 2011b). Carbon emissions in the drawdown area are poorly understood,
317 especially in regulated and dammed rivers. This study fills the knowledge gap and adds
318 to our understanding of the ecological impacts of hydropower exploitation. Under water
319 level fluctuation induced by reservoir operation, variable oxygen conditions and
320 methane production may also affect the mercury cycle in the drawdown area and
321 thereby the release of methylmercury (a bioaccumulative environmental toxicant) to the
322 river (Marvin-DiPasquale et al., 2009), a subject deserving of further study.
323
324 **5 Conclusions**
325 In dammed rivers, sediment deposited islands are widely distributed in sidebays and are
326 potential hotspots of methane emission to the atmosphere. In this study, high methane
327 fluxes were only observed at the island center, while a ring-like zone of low methane
328 emission or even sink was found in the drawdown area around the island edge. We
329 attribute this spatial heterogeneity of methane emissions to hyporheic exchange
330 between the reservoir and island. Under reservoir operation, frequent water level
331 fluctuations drove hyporheic exchange, creating oxygen gradients along the hyporheic
332 flowpath. These oxygen gradients affected the microbial communities associated with
333 methane production and consumption, producing the spatial heterogeneity in methane
334 emissions across sediment-deposited islands. This study will help us to evaluate the
335 global warming effects of hydropower systems.
336
337

Data availability

The data presented here can be obtained upon request to Wenqing Shi (wqshi@nhri.cn).

Author contribution

Qiuwen Chen designed the research; Wenqing Shi, Yuyu Ji and Yuchen Chen performed the research; Cheng Chen and Juhua Yu contributed new reagents/analytic tools; Qiuwen Chen and Wenqing Shi analyzed the data; Jianyun Zhang and Bryce R. Van Dam contributed significant discussions and inputs; Wenqing Shi and Qiuwen Chen wrote the paper with input from all authors.

Competing interests

The authors declare that they have no conflict of interest.

Acknowledgements

Funding for this study was provided by the National Nature Science Foundation of China (No. 91547206, 51425902, 51709181 and 51709182).

References

Bastviken, D., Tranvik, L. J., Downing, J. A., Crill, P. M., and Enrich-Prast, A.: Freshwater methane emissions offset the continental carbon sink, Science, 331, 50-50, 10.1126/science.1196808, 2011.

Boano, F., Revelli, R., and Ridolfi, L.: Reduction of the hyporheic zone volume due to the stream-aquifer interaction, Geophys. Res. Lett., 35, 2008.

Bonalumi, M., Anselmetti, F. S., Wüest, A., and Schmid, M.: Modeling of temperature and turbidity in a natural lake and a reservoir connected by pumped-storage operations, *Water Resour. Res.*, 48, 10.1029/2012wr011844, 2012.

Borrel, G., Jezequel, D., Biderre-Petit, C., Morel-Desrosiers, N., Morel, J. P., Peyret, P., Fonty, G., and Lehours, A. C.: Production and consumption of methane in freshwater lake ecosystems, Res Microbiol, 162, 832-847, DOI 10.1016/j.resmic.2011.06.004, 2011.

Butman, D., and Raymond, P. A.: Significant efflux of carbon dioxide from streams and rivers in the United States, Nature Geoscience, 4, 839-842, 2011.

Butturini, A., Guarch, A., Romaní, A., Freixa, A., Amalfitano, S., Fazi, S., and Ejarque, E.: Hydrological conditions control in situ DOM retention and release along a Mediterranean river, Water research, 99, 33-45, 2016.

Cardenas, M. B., and Wilson, J. L.: Exchange across a sediment-water interface with ambient groundwater discharge, Journal of hydrology, 346, 69-80, 2007.

Cardenas, M. B., and Markowski, M. S.: Geoelectrical imaging of hyporheic exchange and mixing of river water and groundwater in a large regulated river, Environmental

375 Science & Technology, 45, 1407-1411, 2010.
376 Chamberlain, S. D., Gomez-Casanovas, N., Walter, M. T., Boughton, E. H., Bernacchi,
377 C. J., DeLucia, E. H., Groffman, P. M., Keel E. W., and Sparks, J. P.: Influence of
378 transient flooding on methane fluxes from subtropical pastures. Journal of
379 Geophysical Research: Biogeosciences, 121, 965-977 2016.
380 Chen, H., Yuan, X., Chen, Z., Wu, Y., Liu, X., Zhu, D., Wu, N., Zhu, Q., Peng, C., Li,
381 W.: Methane emissions from the surface of the Three Gorges Reservoir. Journal of
382 Geophysical Research: Atmospheres, 116, D21, 2011.
383 DelSontro, T., McGinnis, D. F., Sobek, S., Ostrovsky, I., and Wehrli, B.: Extreme
384 methane emissions from a Swiss hydropower reservoir: contribution from bubbling
385 sediments, Environmental Science & Technology, 44, 2419-2425, 2010.
386 DelSontro, T., Kunz, M. J., Kempter, T., Wüest, A., Wehrli, B., and Senn, D. B.: Spatial
387 heterogeneity of methane ebullition in a large tropical reservoir, Environmental
388 Science & Technology, 45, 9866-9873, 2011.
389 Duchemin, E., Lucotte, M., and Canuel, R.: Comparison of static chamber and thin
390 boundary layer equation methods for measuring greenhouse gas emissions from large
391 water bodies §, Environmental Science & Technology, 33, 350-357, 1999.
392 Dumont, M. G., Murrell, J. C.: Stable isotope probing-linking microbial identity to
393 function. Nature Reviews Microbiology, 3(6), 499, 2005.
394 Gerecht, K. E., Cardenas, M. B., Guswa, A. J., Sawyer, A. H., Nowinski, J. D., and
395 Swanson, T. E.: Dynamics of hyporheic flow and heat transport across a bed-to-bank
396 continuum in a large regulated river, Water Resources Research, 47, 2011.

397 Glatzel, S., Well, R.: Evaluation of septum-capped vials for storage of gas samples
398 during air transport. Environmental Monitoring and Assessment, 136, 307-311, 2008.
399 Hester, E. T., Young, K. I., and Widdowson, M. A.: Mixing of surface and groundwater
400 induced by riverbed dunes: Implications for hyporheic zone definitions and pollutant
401 reactions, Water Resources Research, 49, 5221-5237, 10.1002/wrcr.20399, 2013.
402 Hu, Y., and Cheng, H.: The urgency of assessing the greenhouse gas budgets of
403 hydroelectric reservoirs in China, Nature Climate Change, 3, 708, 2013.
404 Hucks Sawyer, A., Bayani Cardenas, M., Bomar, A., and Mackey, M.: Impact of dam
405 operations on hyporheic exchange in the riparian zone of a regulated river, Hydrol
406 Process, 23, 2129-2137, 2009.
407 Immerzeel, W., Rutten, M., and Droogers, P.: Spatial downscaling of TRMM
408 precipitation using vegetative response on the Iberian Peninsula, Remote Sens
409 Environ, 113, 362-370, 2009.
410 Klupfel, L., Piepenbrock, A., Kappler, A., and Sander, M.: Humic substances as fully
411 regenerable electron acceptors in recurrently anoxic environments, Nat Geosci, 7,
412 195-200, 10.1038/NGEO2084, 2014.
413 Li, J. P., Dong, S. K., Liu, S. L., Yang, Z. F., Peng, M. C., and Zhao, C.: Effects of
414 cascading hydropower dams on the composition, biomass and biological integrity of
415 phytoplankton assemblages in the middle Lancang-Mekong River, Ecol Eng, 60,
416 316-324, 10.1016/j.ecoleng.2013.07.029, 2013.
417 Ma, K., and Lu, Y.: Regulation of microbial methane production and oxidation by
418 intermittent drainage in rice field soil, Fems Microbiol Ecol, 75, 446-456,

10.1111/j.1574-6941.2010.01018.x, 2011.

Maavara, T., Parsons, C. T., Ridenour, C., Stojanovic, S., Durr, H. H., Powley, H. R., and Van Cappellen, P.: Global phosphorus retention by river damming, P Natl Acad Sci USA, 112, 15603-15608, 10.1073/pnas.1511797112, 2015.

Maeck, A., DelSontro, T., McGinnis, D. F., Fischer, H., Flury, S., Schmidt, M., Fietzek, P., and Lorke, A.: Sediment trapping by dams creates methane emission hot spots, Environmental Science & Technology, 47, 8130-8137, 10.1021/es4003907, 2013.

Marvin-DiPasquale, M., Lutz, M. A., Brigham, M. E., Krabbenhoft, D. P., Aiken, G. R., Orem, W. H., and Hall, B. D.: Mercury cycling in stream ecosystems. 2. Benthic methylmercury production and bed sediment-pore water partitioning, Environmental Science & Technology, 43, 2726-2732, 2009.

Mekong River Commision. available at: https://www. mrcmekong.org/mekong-basin/physiography/, 2018

Nazaries, L., Murrell, J. C., Millard, P., Baggs, L., and Singh, B. K.: Methane, microbes and models: fundamental understanding of the soil methane cycle for future predictions. Environmental Microbiology, 15, 2395-2417. 2013.

Naranjo, R. C., Niswonger, R. G., and Davis, C. J.: Mixing effects on nitrogen and oxygen concentrations and the relationship to mean residence time in a hyporheic zone of a riffle-pool sequence, Water Resources Research, 51, 7202-7217, 10.1002/2014WR016593, 2015.

Philip, J.: Approximate analysis of falling-head lined borehole permeameter, Water Resources Research, 29, 3763-3768, 1993.

441 Ran, L., Lu, X., Sun, H., Han, J., Li, R., and Zhang, J.: Spatial and seasonal variability
442 of organic carbon transport in the Yellow River, China, Journal of Hydrology, 498,
443 76-88, 2013.
444 Rubol, S., Manzoni, S., Bellin, A., and Porporato, A.: Modeling soil moisture and
445 oxygen effects on soil biogeochemical cycles including dissimilatory nitrate
446 reduction to ammonium (DNRA), Advances in water resources, 62, 106-124, 2013.
447 Schwarz, J. I. K., Eckert, W., Conrad, R.: Response of the methanogenic microbial
448 community of a profundal lake sediment (Lake Kinneret, Israel) to algal deposition.
449 Limnol. Oceanogr, 2008, 53(1), 113-121.
450 Seitzinger, S., Harrison, J., Dumont, E., Beusen, A. H., and Bouwman, A.: Sources and
451 delivery of carbon, nitrogen, and phosphorus to the coastal zone: An overview of
452 Global Nutrient Export from Watersheds (NEWS) models and their application,
453 Global Biogeochem Cy, 19, 2005.
454 Shi, W., Pan, G., Chen, Q., Song, L., Zhu, L., and Ji, X.: Hypoxia remediation and
455 methane emission manipulation using surface oxygen nanobubbles. Environmental
456 Science & Technology, 52, 8712-8717. 2018
457 Smith, L. K., Lewis, W. M., Chanton, J. P., Cronin, G., and Hamilton, S. K.: Methane
458 emissions from the Orinoco River floodplain, Venezuela, Biogeochemistry, 51, 113-
459 140, 2000.
460 Smith, K. R., Desai, M. A., Rogers, J. V., and Houghton, R. A.: Joint CO_2 and CH_4
461 accountability for global warming, Proceedings of the National Academy of Sciences,
462 110, E2865-E2874, 2013.

463 Sobek, S., DelSontro, T., Wongfun, N., and Wehrli, B.: Extreme organic carbon burial
464 fuels intense methane bubbling in a temperate reservoir, Geophys Res Lett, 39, Artn
465 L0140110.1029/2011gl050144, 2012.
466 Syvitski, J. P., Vörösmarty, C. J., Kettner, A. J., and Green, P.: Impact of humans on the
467 flux of terrestrial sediment to the global coastal ocean, science, 308, 376-380, 2005.
468 Thornton, K. W., Kimmel, B. L., and Payne, F. E.: Reservoir limnology: ecological
469 perspectives, John Wiley & Sons, 1990.
470 Toffolon, M., Siviglia, A., and Zolezzi, G.: Thermal wave dynamics in rivers affected
471 by hydropeaking, Water Resources Research, 46, Artn W08536
472 10.1029/2009wr008234, 2010.
473 Tonina, D., and Buffington, J. M.: Effects of stream discharge, alluvial depth and bar
474 amplitude on hyporheic flow in pool-riffle channels, Water Resources Research, 47,
475 2011.
476 Van Dam, B. R., Tobias, C., Holbach, A., Paerl, H. W., Zhu, G. W.: CO_2 limited
477 conditions favor cyanobacteria in a hypereutrophic lake: An empirical and theoretical
478 stable isotope study, Limnology and Oceanography. 2018.
479 https://doi.org/10.1002/lno.10798
480 Veldkamp, E., Koehler, B., and Corre, M. D.: Indications of nitrogen-limited methane
481 uptake in tropical forest soils, Biogeosciences, 10, 5367-5379, 2013.
482 Wang, C., Liu, S. L., Zhao, Q. H., Deng, L., and Dong, S. K.: Spatial variation and
483 contamination assessment of heavy metals in sediments in the Manwan Reservoir,
484 Lancang River, Ecotox Environ Safe, 82, 32-39, 10.1016/j.ecoenv.2012.05.006, 2012.

485 Wang, J. M., Murphy, J. G., Geddes, J. A., Winsborough, C. L., Basiliko, N., and
486 Thomas, S. C.: Methane fluxes measured by eddy covariance and static chamber
487 techniques at a temperate forest in central Ontario, Canada, Biogeosciences, 10,
488 4371-4382, 2013.
489 Watanabe, T., Kimura, M., and Asakawa, S.: Dynamics of methanogenic archaeal
490 communities based on rRNA analysis and their relation to methanogenic activity in
491 Japanese paddy field soils, Soil Biol Biochem, 39, 2877-2887,
492 10.1016/j.soilbio.2007.05.030, 2007.
493 Wilkinson, J., Maeck, A., Alshboul, Z., and Lorke, A.: Continuous seasonal river
494 ebullition measurements linked to sediment methane formation, Environmental
495 Science & Technology, 49, 13121-13129, 2015.
496 Wuebbles, D. J., and Hayhoe, K.: Atmospheric methane and global change, Earth-Sci
497 Rev, 57, 177-210, 2002.
498 Yang, L., Lu, F., Wang, X., Duan, X., Song, W., Sun, B., Zhang, Q., and Zhou, Y.:
499 Spatial and seasonal variability of diffusive methane emissions from the Three
500 Gorges Reservoir, Journal of Geophysical Research: Biogeosciences, 118, 471-481,
501 2013.
502 Zarnetske, J. P., Haggerty, R., Wondzell, S. M., and Baker, M. A.: Labile dissolved
503 organic carbon supply limits hyporheic denitrification, Journal of Geophysical
504 Research: Biogeosciences, 116, 2011a.
505 Zarnetske, J. P., Haggerty, R., Wondzell, S. M., and Baker, M. A.: Labile dissolved
506 organic carbon supply limits hyporheic denitrification, Journal of Geophysical

507 Research, 116, 10.1029/2011jg001730, 2011b.

508

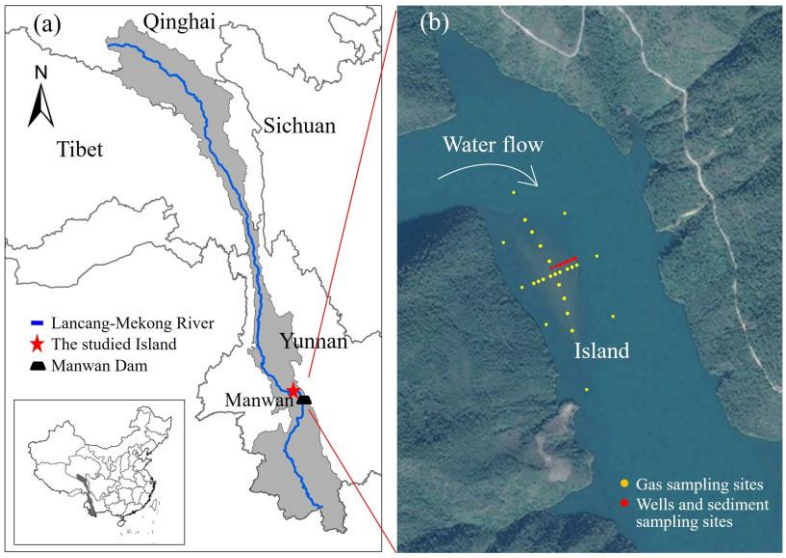

509

510 **Fig. 1** Map of the studied island in Manwan reservoir, Lancang-Mekong River. (a) The

511 island site in the river; (b) The monitoring wells, sediment and gas sampling sites on

512 the island.

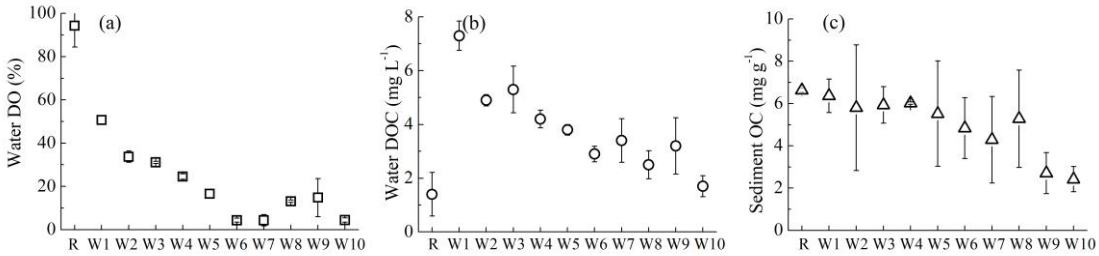

513

514 **Fig. 2** Physicochemical properties of the island and reservoir, including water (a) DO,

515 (b) DOC, and (c) sediment OC. DO = dissolved oxygen, DOC = dissolved oxygen

516 carbon, OC = organic carbon, R = reservoir, W = monitoring wells. Error bars indicate

517 standard deviations.

518

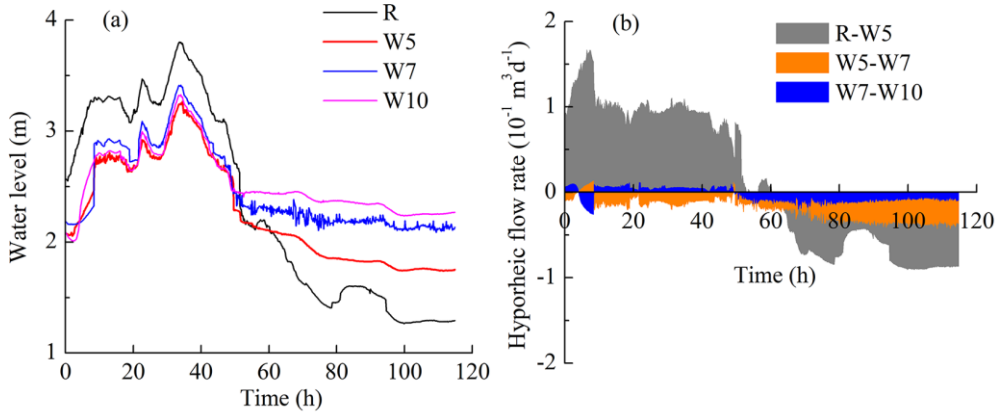

519

520 **Fig. 3** Vertical water level fluctuation (a) and horizontal hyporheic flow rate (b). R =

521 reservoir, W = monitoring wells. Positive fluxes indicate net flow from the reservoir to

522 island, whereas negative values indicate net flow from the island to reservoir.

523

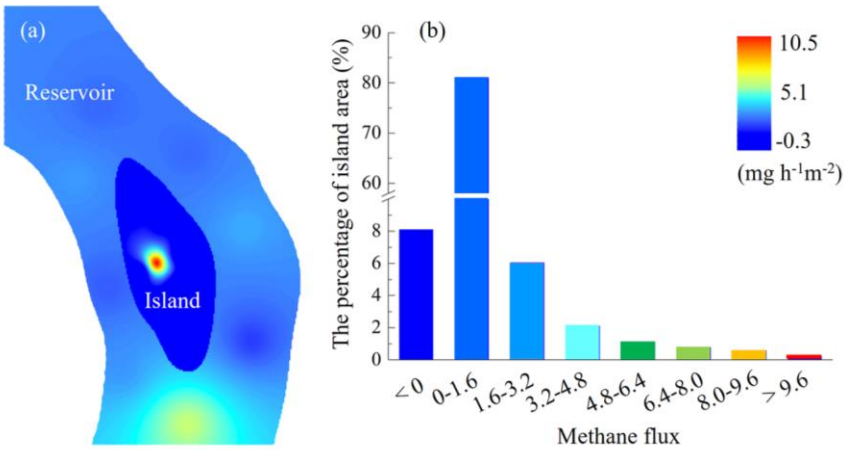

524

525 **Fig. 4** Methane emissions from the island and reservoir. (a) Spatial pattern of methane

526 emissions; (b) Percentage of the island area emitting methane at a certain flux. Methane

527 fluxes were interpolated separately for the island and reservoir.

528

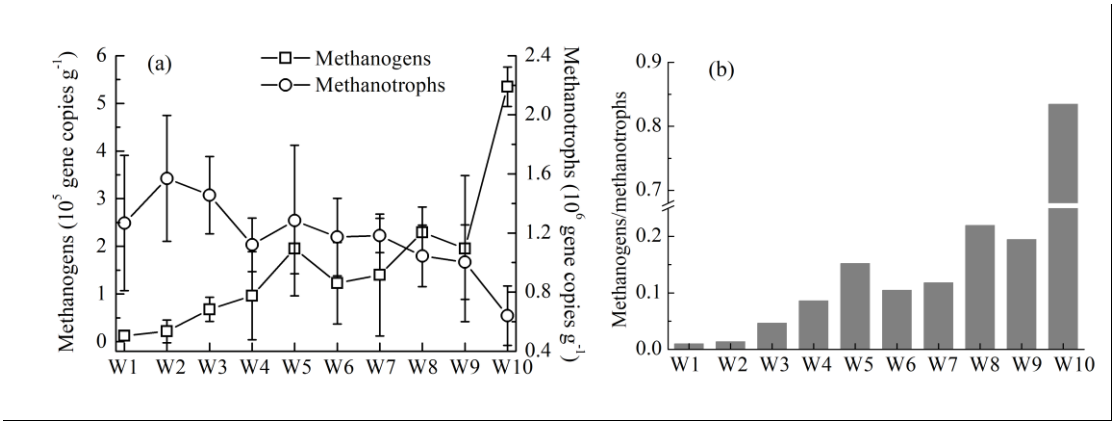

Fig. 5 Abundances of sediment methanogens and methanotrophs in the island. (a) Spatial patterns of methanogen and methanotroph abundances across the island; (b) The ratio of methanogen to methanotroph abundance at each site. W= monitoring wells. Error bars indicate standard deviations.

Fig. S1 The river impoundment formed islands in the Lancang-Mekong River. There were about 33 sediment-deposited islands, of which 81.8% are located at the convex bank (a), and 18.2% at the concave bank (b).

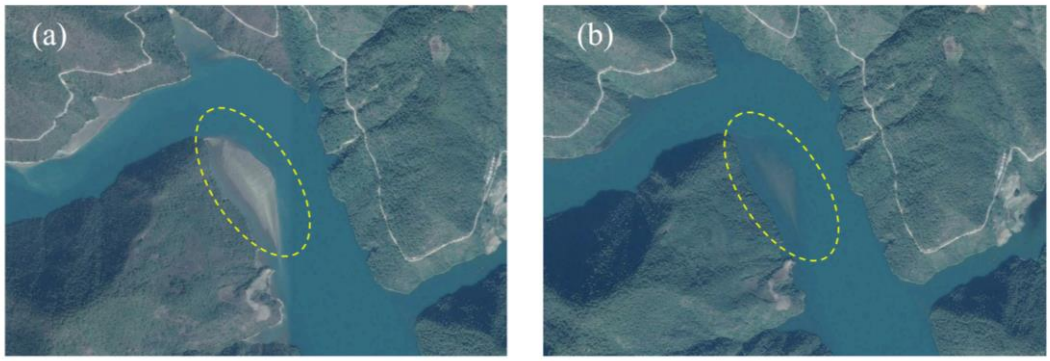

Fig. S2 Island image before (a) and after (b) flooding under reservoir operation.

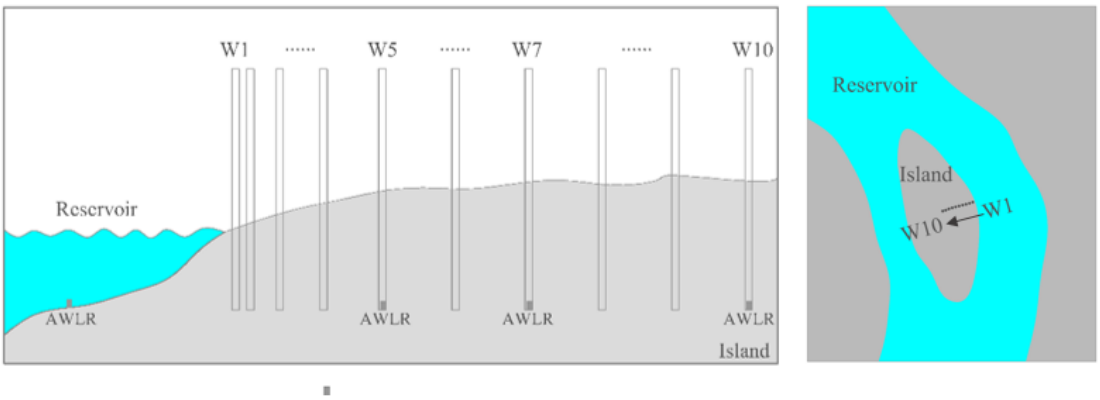

Fig. S3 Monitoring wells established from the island edge to the center. Sediment samples were collected adjacent to each well.

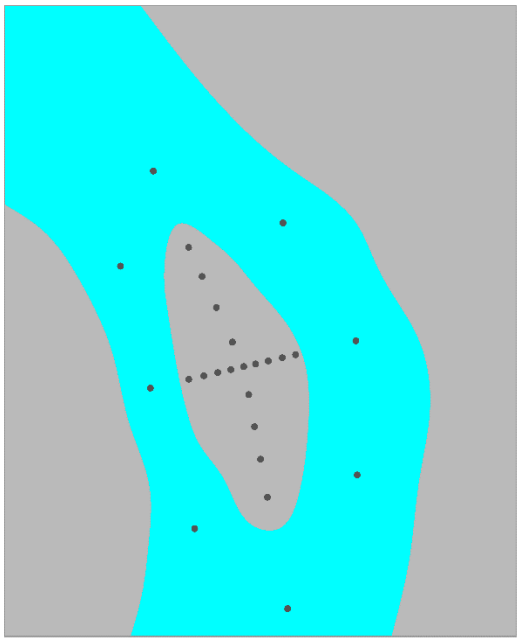

Fig. S4 Sampling sites for methane flux analyses in the island and reservoir, including eight sites in the reservoir and seventeen sites on the island.

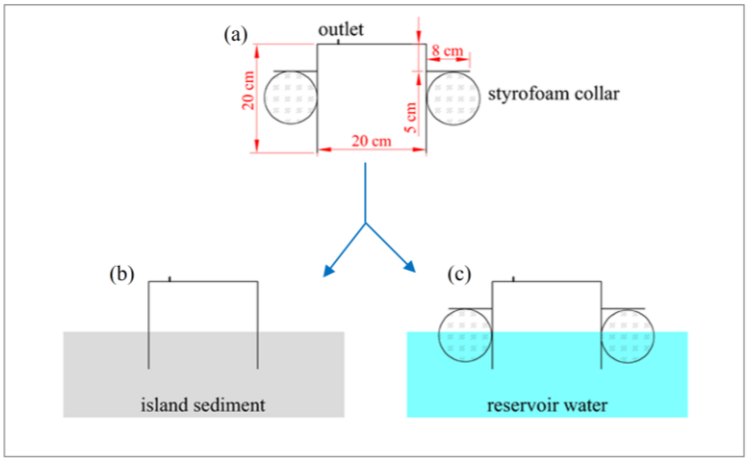

Fig. S5 Bifunctional static chambers (a) for methane flux analyses across the sediment-air interface in the island (b) and water-air interface in the reservoir (c). Styrofoam collar was removable.

Table S1 The data about methane fluxes at each sampling site

Sites		The concentration in the chamber ($\times10^{-6}$ mol/L)					Flux ($\times10^{-6}$ mol/h)	Flux ($\times10^{-6}$ mol/h m^2)	Flux (mg/h m^2)	Average flux (mg/h m^2)
		0 min	10 min	20 min	30 min	40 min				
R1	Rep-1	0.452	0.773	1.174	1.375	1.656	1.806	57.5	0.92	1.07
	Rep-2	0.641	0.921	1.280	1.680	2.160	2.279	72.6	1.16	
	Rep-3	0.541	1.106	1.272	1.637	2.103	2.193	69.8	1.12	
R2	Rep-1	0.797	0.887	1.232	1.778	2.081	2.075	66.1	1.06	1.13
	Rep-2	1.166	1.431	1.722	2.112	2.778	2.343	74.6	1.19	
	Rep-3	0.823	0.869	1.197	3.825	4.273	NA	NA	NA	
R3	Rep-1	0.678	1.075	1.809	2.243	3.264	3.804	121.1	1.94	2.10
	Rep-2	0.822	1.261	2.282	2.702	3.704	4.323	137.7	2.20	
	Rep-3	1.243	1.543	2.246	2.969	4.043	4.216	134.3	2.15	
R4	Rep-1	0.573	0.660	0.759	1.018	1.189	0.954	30.4	0.49	0.39
	Rep-2	0.390	0.553	0.665	0.797	0.829	0.673	21.4	0.34	
	Rep-3	0.476	0.622	0.762	0.863	0.909	0.665	21.2	0.34	
R5	Rep-1	1.867	2.871	4.802	6.432	8.739	10.383	330.7	5.29	5.47
	Rep-2	1.294	2.554	4.565	6.582	9.349	12.082	384.8	6.16	
	Rep-3	1.188	2.165	4.289	4.913	7.935	9.745	310.4	4.97	
R6	Rep-1	0.493	1.175	1.608	2.142	2.678	3.203	102.0	1.63	1.84
	Rep-2	0.881	1.411	1.881	2.751	3.561	4.021	128.1	2.05	
	Rep-3	0.677	1.432	1.381	2.988	3.463	NA	NA	NA	
R7	Rep-1	0.388	0.802	0.923	1.224	1.482	1.566	49.9	0.80	0.84
	Rep-2	0.653	0.876	1.875	1.896	2.165	NA	NA	NA	
	Rep-3	0.794	0.930	1.420	1.609	1.902	1.737	55.3	0.89	
R8	Rep-1	0.971	1.626	2.515	3.401	4.015	4.718	150.3	2.40	1.84
	Rep-2	0.879	0.997	1.377	1.995	2.469	2.508	79.9	1.28	
	Rep-3	0.726	0.726	1.543	1.945	2.807	3.605	114.8	1.84	
1	Rep-1	0.463	0.434	0.358	0.295	0.200	-0.399	-12.7	-0.20	-0.21
	Rep-2	0.454	0.414	0.358	0.255	0.157	-0.452	-14.4	-0.23	
	Rep-3	0.386	0.314	0.258	0.214	0.139	-0.356	-11.3	-0.18	
2	Rep-1	0.878	1.213	1.556	2.009	2.810	2.796	89.0	1.42	1.26
	Rep-2	0.784	0.970	1.432	1.945	2.442	2.575	82.0	1.31	
	Rep-3	0.993	1.187	1.534	1.898	2.358	2.065	65.8	1.05	
3	Rep-1	1.068	1.483	2.425	3.567	4.738	5.654	180.1	2.88	2.78
	Rep-2	1.282	1.919	2.799	3.304	4.482	4.671	148.8	2.38	
	Rep-3	1.482	1.949	2.876	3.967	5.519	6.055	192.8	3.09	
4	Rep-1	2.893	6.897	8.251	12.608	16.811	20.13	641.1	10.26	10.41
	Rep-2	3.892	7.996	10.451	15.906	17.211	20.73	660.2	10.56	
	Rep-3	1.278	2.301	4.061	5.868	8.291	NA	NA	NA	
5	Rep-1	0.786	NA	2.784	4.324	NA	NA	NA	NA	4.27
	Rep-2	0.876	1.805	3.180	4.625	5.769	7.564	240.9	3.85	
	Rep-3	1.069	2.075	3.208	5.141	7.203	9.201	293.0	4.69	
6	Rep-1	1.221	1.519	1.697	1.875	1.933	1.068	34.0	0.54	0.49

	Rep-2	0.782	0.819	0.999	1.153	1.338	0.868	27.6	0.44	
	Rep-3	1.887	1.267	1.756	2.154	2.375	NA	NA	NA	
7	**Rep-1**	0.456	0.476	0.481	0.493	0.507	0.071	2.3	0.04	0.03
	Rep-2	0.479	0.489	0.499	0.505	0.515	0.05	1.6	0.03	
	Rep-3	0.578	0.587	0.602	0.611	0.62	0.065	2.1	0.03	
8	**Rep-1**	0.399	0.408	0.417	0.422	0.428	0.043	1.4	0.02	0.03
	Rep-2	0.456	0.471	0.482	0.503	0.512	0.086	2.7	0.04	
	Rep-3	0.488	0.497	0.505	0.517	0.519	0.049	1.6	0.02	
9	**Rep-1**	0.678	0.6768	0.676	0.675	0.6745	-0.005	-0.2	0.00	-0.01
	Rep-2	0.544	0.536	0.531	0.528	0.521	-0.032	-1.0	-0.02	
	Rep-3	0.487	0.483	0.48	0.475	0.472	-0.023	-0.7	-0.01	
10	**Rep-1**	0.661	0.67	0.678	0.683	0.687	0.039	1.2	0.02	0.02
	Rep-2	0.495	0.502	0.506	0.512	0.519	0.035	1.1	0.02	
	Rep-3	0.785	0.791	0.795	0.802	0.809	0.0355	1.1	0.02	
11	**Rep-1**	0.555	0.5545	0.5538	0.5535	0.5528	-0.003	-0.1	0.00	0.00
	Rep-2	0.453	0.454	0.454	0.455	0.456	0.004	0.1	0.00	
	Rep-3	0.768	0.745	0.755	0.777	0.815	NA	NA	NA	
12	**Rep-1**	0.787	1.199	1.443	2.108	2.588	2.707	86.2	1.38	1.12
	Rep-2	0.722	0.805	1.119	1.403	1.844	1.705	54.3	0.87	
	Rep-3	0.477	0.674	0.846	0.876	1.532	NA	NA	NA	
13	**Rep-1**	0.491	1.118	1.694	2.171	2.847	3.46	110.2	1.76	1.61
	Rep-2	0.493	1.015	1.290	1.965	2.390	2.85	90.8	1.45	
	Rep-3	NA	0.564	NA	0.762	1.438	NA	NA	NA	
14	**Rep-1**	0.393	0.444	0.477	0.521	0.532	0.021	0.7	0.01	0.01
	Rep-2	0.420	0.425	0.430	NA	0.439	0.029	0.9	0.01	
	Rep-3	0.422	0.427	0.432	0.435	0.440	0.0265	0.8	0.01	
15	**Rep-1**	0.754	0.733	0.695	0.677	0.644	-0.166	-5.3	-0.08	-0.05
	Rep-2	0.472	0.463	0.455	0.447	0.435	-0.054	-1.7	-0.03	
	Rep-3	0.511	0.493	0.475	0.457	0.447	-0.098	-3.1	-0.05	
16	**Rep-1**	0.567	0.540	0.525	0.511	0.503	-0.094	-3.0	-0.05	-0.04
	Rep-2	0.853	0.840	0.835	0.821	0.809	-0.064	-2.0	-0.03	
	Rep-3	0.454	0.440	0.435	0.411	0.398	-0.085	-2.7	-0.04	
17	**Rep-1**	0.263	0.564	0.672	0.675	0.785	NA	NA	NA	0.01
	Rep-2	0.567	0.570	0.572	0.574	0.575	0.012	0.4	0.01	
	Rep-3	0.368	0.370	0.375	0.377	0.381	0.02	0.6	0.01	